Impaired adipose anabolism in pancreatic cancer cachexia is reversed by HuR inhibition

Paige C. Arneson-Wissink[1,2], Katherine Pelz[1,3], Beth Worley[1], Heike Mendez [1,2], Peter Pham[1,2], Parham Diba[1,2], Peter R. Levasseur [1,2], Grace McCarthy [1,3], Alex Chitsazan[4], Jonathan R. Brody [1,3,5], Aaron J. Grossberg*[1,2,4,5]

[1]Brenden-Colson Center for Pancreatic Care, Oregon Health & Science University, Portland, OR

[2]Department of Radiation Medicine, Oregon Health & Science University, Portland, OR

[3]Department of Surgery, Oregon Health & Science University, Portland, OR

[4]Cancer Early Detection Advanced Research Center, Oregon Health & Science University, Portland, OR

[5]Department of Cell, Developmental, and Cancer Biology, Oregon Health & Science University, Portland, OR

***Corresponding Author**: Aaron J. Grossberg, 3181 SW Sam Jackson Park Rd Mail Code L481, Oregon Health and Science University, Portland, OR, 97239, 503-494-9945, grossber@ohsu.edu

ABSTRACT

Background: Cachexia is defined by chronic loss of fat and muscle, is a frequent complication of pancreatic ductal adenocarcinoma (PDAC), and negatively impacts patient outcomes. Nutritional supplementation cannot fully reverse tissue wasting, and the mechanisms underlying this phenotype are unclear. This work aims to define the relative contributions of catabolism and anabolism to adipose wasting in PDAC-bearing mice. Human antigen R (HuR) is an RNA-binding protein recently shown to suppress adipogenesis. We hypothesize that fat wasting results from a loss of adipose anabolism driven by increased HuR activity in adipocytes of PDAC-bearing mice.

Methods: Adult C57BL/6J mice received orthotopic PDAC cell (*Kras*^{G12D}*; p53*$^{R172H/+}$*; Pdx1-cre*) (PDAC) or PBS (sham) injections. Mice exhibiting moderate cachexia (9 days after injection) were fasted for 24h, or fasted 24h and refed 24h before euthanasia. A separate cohort of PDAC mice were treated with an established HuR inhibitor (KH-3, 100 mg/kg) and subjected to the fast/refeed paradigm. We analyzed body mass, gross fat pad mass, and adipose tissue mRNA expression. We quantified lipolytic rate as the normalized quantity of glycerol released from 3T3-L1 adipocytes *in vitro*, and gonadal fat pads (gWAT) *ex vivo*.

Results: 3T3-L1 adipocytes treated with PDAC cell conditioned media (CM) had lower expression of lipolysis and lipogenesis genes than control cells, and did not display elevated lipolysis as measured by liberated glycerol. PDAC gWAT cultured *ex vivo* displayed decreased lipolysis compared to sham gWAT (-54.7%). PDAC and sham mice lost equivalent fat mass after a 24h fast, however, PDAC mice could not restore inguinal fat pads (iWAT) (-40.5%) or gWAT (-31.8%) mass after refeeding. RNAseq revealed 572 differentially expressed genes in gWAT from PDAC compared to sham mice. Downregulated genes (n=126) were associated

with adipogenesis (adj p=0.05), and expression of adipogenesis master regulators *Pparg* and *Cebpa* were reduced in gWAT from PDAC mice. Immunohistochemistry revealed increased HuR staining in gWAT (+74.9%) and iWAT (+41.2%) from PDAC mice. Inhibiting HuR binding restored lipogenesis in refed animals with a concomitant increase in iWAT mass (+131.7%). **Conclusions:** Our work highlights deficient adipose anabolism as a driver of reduced lipid content in 3T3-L1 adipocytes treated with PDAC conditioned media and PDAC mice. The small molecule KH-3, which disrupts HuR binding, restored adipose anabolism in PDAC mice. This highlights HuR as a potentially targetable regulatory node for adipose anabolism in cancer cachexia.

Key words: pancreatic ductal adenocarcinoma, cachexia, adipose, adipogenesis, HuR

INTRODUCTION

Cancer-associated cachexia is a wasting condition characterized by systemic inflammation, progressive weight loss, and atrophy of white adipose tissue (WAT) and skeletal muscle [1, S1-2]. In addition to physical deterioration, individuals with cachexia also exhibit fatigue, anorexia, and cognitive decline [1, S1-3], which contribute significantly to reductions in quality of life, ability to tolerate chemotherapy or surgery, and patient mortality [2, 3, S4-6]. Cachexia is estimated to be the direct cause of death in 20-30% of cancer patients [2, S4], and among all malignancies, pancreatic ductal adenocarcinoma (PDAC) is the most highly associated with cachexia, with an estimated 83% of patients suffering from this condition [4, S7-8]. Despite much of cachexia research focusing on improving skeletal muscle mass, a retrospective study of patients with PDAC revealed that fat loss alone is associated with equally poor outcomes as combined muscle and fat mass loss [5]. Additionally, current cachexia clinical trials center around weight maintenance or gain as a primary endpoint. This highlights the importance of understanding the drivers of adipose tissue loss in cachexia.

Cachexia arises when energy catabolism exceeds anabolism, leading to unsustainable levels of fat mobilization and muscle depletion. Multiple factors are known to enhance catabolism, including decreased secretion of anabolic hormones, and altered metabolism of protein, carbohydrate, and lipid substrates [6]. Current work suggests that inflammation drives metabolic abnormalities in cachexia [7, S7]. Pro-inflammatory cytokine activity increases during cancer progression [8, 9] and systemic inflammation can contribute to wasting by inducing hypercatabolism in muscle and adipose tissue [6, 10-12]. Existing literature highlights elevated rates of lipolysis and adipose browning as the primary forces underlying adipose tissue wasting [13, 14]. Browning, in particular, appears to exert a double effect in cachexia by

both reducing lipid stores and increasing energy expenditure [14]. However, impaired anabolic processes, like adipogenesis and lipogenesis, also contribute to adipose tissue loss [15]. Targeting peroxisome proliferator-activated receptor gamma (PPARG), a transcriptional control point of adipogenesis, with the agonist rosiglitazone was sufficient to improve fat and muscle mass retention in mice with lung cancer [16]. Tumor-derived factors are also capable of impairing adipogenesis in cultured 3T3L-1 adipocytes [17, 18].

RNA-binding proteins (RBPs) are essential in governing biogenesis, stabilization, translation, and decay of mRNA transcripts [19, 20]. In adipose tissue, several RBPs are documented to regulate alternative splicing [21-23], control of key adipogenic transcription factors [24], and the translation efficiency of proteins involved in browning [25]. Until recently, the function of most RBPs in adipocytes was largely unexplored. The RBP human antigen R (HuR), encoded by the embryonic lethal abnormal vision-like 1 (*ELAVL1*) gene, regulates the expression of genes involved in inflammation, stress response, and apoptosis [26]. Although HuR likely exerts complex effects in the context of both PDAC and cachexia, we selected HuR as a target of interest because recent work showed that it is a repressor of adipogenesis in both white and brown adipose tissues [27]. Our goal was to elucidate the relative contributions of enhanced catabolism and impaired anabolism on fat wasting by investigating adipose tissue response to different nutritional contexts and HuR inhibition in cachectic mice.

METHODS

Cell culture

KPC PDAC cells

KPC cells expressing pancreas-specific conditional alleles (*Kras*^{G12D}*; p53*$^{R172H/+}$*; Pdx1-cre*) [28] were stored in liquid nitrogen until use and then maintained in RMPI 1640

103 supplemented with 10% FBS, 1mM sodium pyruvate, and 50 U/mL penicillin/streptomycin
104 (Gibco, Gaithersburg, MD) at 37C and 5% CO_2. Conditioned media (CM) was collected from
105 confluent KPC cells grown in DMEM, 1% pen/strep (to accommodate later culturing of 3T3-L1
106 cells) after 24 hours incubation, centrifuged at 1,200 g for 10 min, filtered with a 0.2-μm syringe
107 filter, and used immediately or stored at −80°C.

108 *3T3-L1 adipocytes*

109 3T3-L1 adipocytes (ATCC CL-173) were purchased from ATCC and stored in liquid
110 nitrogen until use. Cells were cultured in preadipocyte expansion media (DMEM, 10% bovine
111 calf serum, 1% pen/strep). Then, cells were plated for differentiation at a density of $2x10^5$
112 cells/6-well dish, or 6.7 $x10^3$ cells/96well dish and maintained in preadipocyte expansion media
113 for 2 days after reaching 100% confluency. Media was changed to adipocyte differentiation
114 media (DMEM, 10% FBS, 1% pen/strep, 1 uM dexamethasone, 0.5 mM IBMX, 1 ug/mL bovine
115 insulin) for 2 days before switching to adipocyte maintenance media (DMEM, 10% FBS, 1%
116 pen/strep, 1 ug/mL bovine insulin) for the duration of the experiment. Cells were cultured for up
117 to 6 days after start of maintenance media to reach complete differentiation. For Oil Red O
118 staining, CM was added in place of adipocyte maintenance media and was supplemented with
119 FBS and insulin for 6 days. For lipolysis assay (media glycerol, qPCR, and western blot), cells
120 were completely differentiated and then changed to control media, KPC conditioned media
121 without insulin or FBS. Isoproterenol (10 uM) was added to media as a positive control.
122 Lipolysis end points were collected at 1, 3, and 24 hours after media change.

123 *Oil red O staining*

124 Diluted Oil Red O stock solution was prepared by mixing concentrated Oil Red O (0.5%
125 Oil Red O in 100% isopropyl alcohol) 6:4 with deionized water. This solution was allowed to

126 stand for 10 minutes at 4C and then filtered immediately before use through a 0.22 um filter.
127 3T3-L1 cells were washed with PBS, then incubated in 4% paraformaldehyde for 30 minutes at
128 room temperature, then washed with deionized water twice. Cells were incubated in 60%
129 isopropyl alcohol for 5 minutes, then treated with diluted Oil Red O solution for 15 minutes.
130 Cells were washed 5 times with deionized water, then red signal was quantified at 490 nm in a
131 plate reader (BioTek).

132 *Glycerol quantification*

133 3T3-L1 adipocyte media was collected and run at a 1:2 dilution, and mouse plasma
134 samples were run undiluted for glycerol quantification according to the manufacturer's
135 instructions (Abcam ab65337). Fresh media and KPC CM alone (no 3T3-L1 exposure) were
136 below the detection limit of the assay.

137 *NEFA quantification*

138 Mouse plasma was run undiluted according to the manufacturer's instructions (Wako
139 Diagnostics NEFA-HR series). mEq/L are the units specified by the assay manufacturer and
140 what is standard reporting in clinical values. mEq/L = mM * |valence charge| . Because NEFAs
141 have a valence charge of -1, mEq/L is equivalent to mM.

142 *Mouse studies*

143 Wildtype C57BL/6J mice (JAX catalog number 000664) were purchased from The
144 Jackson Laboratory (Bar Harbor, ME) and maintained in standard rodent housing at 26°C with
145 12h light/12h dark cycles. Sex is defined in individual figure legends. Animals used for
146 experimentation were 12-15 weeks of age. Mice were individually housed for acclimation for 7
147 days prior to tumor implantation and provided *ad libitum* access to water and food (Rodent diet
148 5001; Purina Mills, St. Louis, MO, USA). Food intake was measured daily. Tumor-bearing

149 animals were euthanized by cardiac puncture under deep isoflurane anesthesia. Studies were
150 conducted in accordance with the U.S. National Institutes of Health Guide for the Care and
151 Use of Laboratory Animals and approved by the Institutional Animal Care and Use Committee
152 of Oregon Health & Science University.

153 *Study-specific manipulations*

154 For fasting studies, mice were transferred to clean cages without food for 24 hours prior
155 to euthanasia or refeeding. Pair-feeding was used on the study days indicated in the figure
156 legends by feeding sham mice the average of the food consumed by PDAC mice the day prior.
157 PDAC mice treated with the HuR inhibitor KH-3, were injected intraperitoneally (100 mg/kg) at
158 6-, 8-, and 10-days post-implantation.

159 *Orthotopic PDAC implantation*

160 Wildtype C57BL/6J mice aged 12-15 weeks received orthotopic PDAC tumor injections
161 (*Kras*^{G12D}*; p53*$^{R172H/+}$*; Pdx1-cre*) or sham injections. PDAC mice were injected with $1x10^6$ KPC
162 cells into the tail of the pancreas parenchyma in a volume of 23ul while sham animals were
163 treated with an equal volume of PBS. Animals were euthanized 10-11 days after tumor
164 implantation. N and sex are defined on a per-study basis in the figure legends.

165 *Echo magnetic resonance imaging body composition*

166 Lean mass, fat mass, total body water, and free water were measured using whole-
167 body magnetic resonance imaging (MRI) (EchoMRI, Houston, TX). Measurements were taken
168 pre-implantation (baseline), pre-fasting and at euthanasia in tumor and sham groups to assess
169 body composition.

170 *Tissue collection and histology*

171 Tissues collected at necropsy were weighed and flash frozen in liquid nitrogen prior to
172 storage at -80C. Tissues for HuR histology were fixed with 4% paraformaldehyde overnight
173 and then transferred to 70% ethanol. Tissues were paraffin-embedded, sectioned, incubated
174 with anti-HuR (1:300 #sc-5261, Santa Cruz) and stained using horseradish peroxidase-
175 conjugated secondary antibody and incubation in 3,3'-diaminobenzidine by the Histopathology
176 Shared Resource Core at OHSU. Whole tissue sections were scanned by the Advanced Light
177 Microscopy Core at OHSU. ZEN Digital Imaging for Light Microscopy (RRID:SCR_013672)
178 was then used to obtain at least five 10x images per tissue. ImageJ software was used to
179 quantify the percent staining for each section (56). All staining was quantified by running color
180 deconvolution on 10x images, applying a standard intensity threshold on the corresponding
181 images, and measuring the percent area covered by the staining.

182 *Ex vivo lipolysis*

183 *Ex vivo* lipolysis assays of adipose explants were performed as previously described
184 [29]. Briefly, gonadal white adipose tissue (gWAT) tissue was collected from ad-lib fed sham
185 and PDAC mice 10 days after tumor implantation. Tissues were cut into approximately 100 mg
186 samples, minced, then incubated in phenol red-free DMEM containing 2% fatty acid free
187 bovine serum albumin at 37°C for 1 hour. Media was collected and snap-frozen. The tissue
188 was transferred to a new dish containing media only or media with 10 uM isoproterenol and
189 incubated for 2 hours at 37C. Media was collected and snap-frozen. Media aliquots were
190 thawed and analyzed for glycerol using Sigma Glycerol Assay Kit (MAK117) according to
191 manufacturer's directions.

192 *Quantitative qRT-PCR*

193 Total RNA was extracted from cell pellets or tissues with the E.Z.N.A. Total RNA Kit II
194 (Omega Bio-Tek Inc., Norcross, GA). cDNA was transcribed with the High-Capacity cDNA
195 Reverse Transcription Kit (Applied Biosystems, Waltham, MA). Quantitative real-time
196 polymerase chain reaction (qPCR) was run on the ABI 7300 (Applied Biosystems) using
197 TaqMan Fast Advanced PCR Master Mix (Applied Biosystems) or SYBR Green Master Mix
198 (Applied Biosystems). The relative expression was calculated using the $\Delta\Delta C_t$ method with
199 gene expression relative to beta actin or 18S.

200 *RNA sequencing*

201 RNA sequencing was performed on total RNA isolated as described above. RNA
202 libraries were prepared and sequenced using the Illumina Nova Seq and HiSeq platform
203 according to the Illumina Tru-Seq protocol (Novogene, Sacramento, CA). Detailed analysis
204 methods are included in the supplement.

205 *Western Blot*

206 3T3-L1 protein was collected by scraping cells into lysis buffer followed by brief
207 sonication. Adipose tissue protein was collected using the Minute Total Protein Extraction Kit
208 (Invent Biotechnologies Inc AT-022) and the manufacturer's protocol. We used BCA assay to
209 determine protein concentration. Approximately twenty micrograms of protein was loaded in
210 each lane and run on 4–12% Bis-Tris NuPAGE gel (Invitrogen). Gels were transferred to
211 polyvinylidene difluoride (PVDF) membranes (Millipore) and blocked with 5% BSA for 1 h.
212 Membranes were incubated with primary antibodies overnight at 4°C with gentle agitation.
213 Blots were then washed with Tris-buffered saline with Tween 20 (TBST) and incubated in
214 secondary antibodies for 1 h prior to imaging (LI-COR Odyssey Imaging System). Ladders
215 used were iBright Pre-stained Protein Ladder (Invitrogen)(HuR blot), and Chameleon 700 Pre-

216 stained Protein Ladder (LI-COR)(all other blots). Primary antibodies: Vinculin (Santa Cruz sc-
217 73614), HuR (Santa Cruz sc-5261), ATGL (Cell Signaling 2138), HSL (Cell Signaling 4107),
218 Phospho-HSL (Ser660) (Cell Signaling 45804), and Phospho-HSL (Ser563) (Cell Signaling
219 4139). Secondary antibodies: Mouse IgG and Rabbit IgG Dylight 680 and 800 (Cell Signaling),
220 goat anti-mouse IgG Alexa Fluor Plus 800 (Invitrogen A32730), and goat anti-mouse IgG Alexa
221 Fluor Plus 647 (Invitrogen A32728).

222 ***Statistical Analysis***

223 Specific statistical tests and sample size for each study is indicated in the figure
224 legends. Error bars in figures show SEM. Statistical analyses were performed using GraphPad
225 Prism (version 9; GraphPad Software Inc), and graphs were built using GraphPad Prism
226 (GraphPad Software Inc) statistical analysis software or R studio (4.2.3) using ggplot (3.5.1). P
227 values are 2 sided with values less than 0.05 regarded as statistically significant.

228 ***Data Availability***

229 Further information and resources, including KPC cells and raw data will be shared
230 upon reasonable request to Aaron J. Grossberg (grossber@ohsu.edu).

231

232 **RESULTS**

233 **Adipocytes suppress lipogenesis in response to PDAC-derived factors**

234 Given a large body of literature suggesting that PDAC cachexia is partly driven by
235 increased lipolysis in the adipose tissue, we tested the effect of PDAC cell-conditioned media
236 (KPC CM) on lipolysis *in vitro* [13, 14, 30]. We treated differentiated 3T3-L1 cells with control
237 maintenance media, or with KPC CM for 6 days. At this time, we observed decreased lipid
238 droplet accumulation by brightfield microscopy, which was confirmed with Oil Red O (**Figure**

239 **1A-B**). Media glycerol levels, a measure of lipolysis, were not elevated in KPC CM-treated
240 cells (**Figure 1C**, **S1A**). Correspondingly, protein markers of lipolysis, including activated
241 (phosphorylated) hormone-sensitive lipase (HSL) and adipose triglyceride lipase (ATGL) were
242 not elevated in KPC CM-treated cells (**Figure 1D-E, S1B-E, S2**) and mRNA levels of lipolysis
243 enzymes *Atgl* and hormone-sensitive lipase (lipase e, *Lipe*) were significantly decreased in
244 KPC CM-treated 3T3-L1 cells (**Figure 1F**). To explain the apparent decrease in lipid
245 accumulation without increased lipolysis, we measured the expression of genes associated
246 with lipogenesis: diacylglycerol O-acyltransferase 1 and 2 (*Dgat1 and Dgat 2),* fatty acid
247 synthase (*Fasn*), lipoprotein lipase (*Lpl*), nuclear receptor subfamily 1 group H member 3
248 (*Nr1h3*), stearoyl-CoA Desaturase 1 (*Scd1*), solute carrier family 2 member 4 (*Slc2a4*), and
249 sterol regulatory element-binding protein 1c (*Srebp1c*). All of these genes were suppressed
250 after 24 hour KPC CM treatment, indicating that the decreased lipid content in 3T3-L1 cells
251 was due to impaired anabolic activity rather than increased catabolic activity (**Figure 1F**).

252 **PDAC is associated with decreased fat pad mass *in vivo***

253 We first sought to assess the effects of pancreatic cancer on metabolism by
254 characterizing tissue physiology in a murine orthotopic PDAC model. 12-week-old C57BL/6J
255 mice with PDAC or sham implantations were fed *ad libitum* with or without a 24h fast once
256 mice reached a moderate cachexia burden (9 days after tumor implantation). Body mass
257 maintained stable among all groups prior to fasting (**Figure 2A**), whereas PDAC mice
258 exhibited a small reduction in food intake (**Figure 2B**) compared to sham controls. Fasting
259 caused a significant reduction in tumor mass compared to *ad libitum*-fed mice **(Figure 2C).**
260 EchoMRI body composition analysis of fat mass demonstrated significant decreases in overall
261 adiposity in PDAC animals from baseline to pre-fast due to cachexia progression and reduction

262 in food intake (**Figure 2D**). As expected, between pre- and post-fast, both PDAC and sham
263 animals lost significant overall adiposity (**Figure 2E**). Terminal fat pad masses (inguinal, iWAT,
264 and gonadal, gWAT) were significantly decreased in both ad lib and fasted conditions as
265 compared to sham mice (**Figure 2F**). PDAC mice were also vulnerable to skeletal muscle
266 mass loss as measured by echoMRI and gastrocnemius muscle tissue mass (**Figure S3**).

267 **PDAC impairs lipolysis and adipogenesis**

268 Based on our findings *in vitro*, we hypothesized that PDAC mice would not exhibit
269 increased lipolysis, which is characteristic of other cachexia models [13, 30]. To assess
270 products of lipolysis in circulation, we measured plasma glycerol and non-esterified fatty acids
271 (NEFAs). Plasma glycerol levels were significantly lower in fasted PDAC mice than in fasted
272 sham mice (**Figure 3A**), while there was no significant difference in plasma NEFA levels
273 between fasted groups (**Figure 3B**). To directly measure the rate of adipose tissue catabolism,
274 we performed an *ex vivo* lipolysis study, using gonadal white adipose tissue (gWAT) collected
275 from sham and PDAC mice. We assessed fat pads both in the presence and absence of the
276 beta-adrenergic agonist isoproterenol (10 uM) to determine baseline and stimulated lipolysis
277 [29]. Baseline and isoproterenol-stimulated glycerol release were significantly decreased in
278 PDAC gWAT (**Figure 3C**), demonstrating that PDAC suppresses, rather than enhances,
279 lipolytic rate and capacity. To further characterize adipose tissue in PDAC mice, we assessed
280 mRNA expression of genes regulating lipolysis and browning in adipose tissue. PDAC mice
281 had suppressed protein and mRNA expression of ATGL and suppressed activation
282 (phosphorylation) of HSL in the gWAT (**Figure 3D,F, S4**). PDAC mice also showed
283 suppressed iWAT and gWAT *Lipe* expression under fasted conditions (**Figure 3D-E**). We
284 observed suppressed browning-associated gene expression in gWAT, including the genes

285 peroxisome proliferator-activated receptor gamma coactivator 1 alpha (*Pgc1a),* protein domain
286 containing 16 (*Prdm16*), and cell death inducing DFFA like effector a (*Cidea*) in PDAC mice in
287 both *ad libitum* fed and fasted conditions. Uncoupling protein 1 (*Ucp1*), which is also
288 associated with browning, was not significantly increased in gWAT or iWAT from PDAC mice
289 (**Figure 3D-E**). Therefore, neither enhanced lipolysis nor browning are significant contributors
290 to adipose loss in this model.

291 **PDAC downregulates pathways associated with adipogenesis**

292 To gain further insights into PDAC metabolism from global gene expression analysis,
293 we performed bulk RNA sequencing (RNAseq) on gWAT from sham and PDAC animals. . In
294 gWAT, we identified a total of 572 differentially expressed genes (DEGs) in PDAC versus
295 sham mice, of which 446 were enriched, and 126 were depleted (**Figure 4A, S5**). Pathway
296 analysis referencing the molecular signatures database (MSigDB) hallmark gene set collection
297 revealed increased expression of gene sets associated with cell cycle control (e.g., E2F
298 targets and G2M checkpoints) and inflammation (e.g. TNFa and JAK/STAT3 signaling) and
299 decreased expression of genes linked to adipogenesis, oxidative phosphorylation, and fatty
300 acid metabolism (**Figure 4B**) [31]. Because inhibition of adipogenesis could provide an
301 alternative mechanism for adipose wasting, we plotted all significant DEGs in the adipogenesis
302 gene set and observed nearly universal depletion of these transcripts in PDAC mice (**Figure**
303 **4C**). We then validated our RNAseq data by performing qPCR on selected adipogenesis-
304 associated DEGs, revealing consistent downregulation of both adipogenesis and lipogenesis
305 genes (**Figure 4D**). We then repeated qPCR in iWAT to determine whether subcutaneous
306 adipose exhibited the same transcriptomic changes. Transcriptional changes in iWAT were
307 less dramatic than in gWAT and did not reach significance, with the exception of *Lpl*, which

308 was significantly decreased in PDAC tissue (**Figure 4E**). Together, these results indicate that
309 suppressed transcriptomic programs associated with adipogenesis could account for
310 decreased adipose tissue during cachexia, in the absence of elevated lipolysis.

311 **Adipose tissue anabolism is impaired in orthotopic PDAC mice after refeeding**

312 Based on our results demonstrating downregulation of adipogenic and lipogenic genes
313 in PDAC mice, we next wanted to confirm whether adipose tissue anabolism is functionally
314 impaired in mice implanted with orthotopic PDAC. To do this, wildtype C57BL/6J mice with
315 PDAC or sham implantations were fed *ad libitum* for 9 days, an established timepoint of active
316 cachexia [32], fasted 24h, and then terminated or allowed to re-feed for 24 h. To control for
317 differences in caloric intake, we used a pair-fed refeeding scheme in which sham mice were
318 refed with the average food consumption of the refed PDAC group. Challenging mice with a
319 24h fast depletes adipose mass in both PDAC and sham mice (**Figure 2D**), enabling us to
320 assess anabolic restoration of fat mass during a 24 h refeeding period. We measured
321 cumulative food intake and daily body mass for the duration of the study (**Figure 5A-B**). 24h
322 fasting followed by 24h refeeding did not impact pancreas tumor mass (**Figure S6**). There
323 were no differences in iWAT or gWAT mass in fasted PDAC versus sham mice (**Figure 5C-D**).
324 However, while sham mice regain significant amounts of gWAT and iWAT mass after
325 refeeding, gWAT and iWAT masses in PDAC mice remain equivalent before and after
326 refeeding (**Figure 5C-D**). Refeeding sham mice caused increased gWAT expression of
327 lipogenic *Fasn* and adipogenic genes *Lep* and *Retn*, while these genes remained suppressed
328 in PDAC gWAT (**Figure 5E**). Refed sham iWAT showed increased *Fasn,* but not adipogenic
329 genes, while PDAC iWAT had suppressed expression of both adipogenic and lipogenic genes
330 (**Figure 5F**). These results confirm that downregulation in pathways mediating adipogenesis

331 are indeed accompanied by impaired adipose tissue anabolism in orthotopic PDAC mice after
332 refeeding.

333 **HuR is highly expressed in orthotopic PDAC fat tissue**

334 Following our observation that adipose tissue anabolism is impaired in PDAC animals,
335 we next sought to understand the mechanism of this phenomenon. We used Ingenuity
336 Pathway Analysis upstream regulator analysis to identify potential candidates that could drive
337 impaired anabolism in PDAC adipose tissue. From the DEGs identified in gWAT of PDAC
338 mice, we found that canonical regulators of adipogenesis, such as troglitazone, fenofibrate,
339 PPARA, and PGC1A, were predicted to be inhibited. Inflammatory cytokines associated with
340 PDAC and cachexia, such as MYD88, IL-6, TNFA, IFNG, and IL-1B, were predicted to be
341 activated. Among other targets that were predicted to be activated but were not typically
342 associated with cachexia was human antigen R (HuR, *ELAVL1*), an RNA-binding protein
343 recently established as a suppressor of adipogenesis [27] (**Figure 6A**). Given the predicted
344 activation of HuR in gWAT and existing literature, we next asked if HuR was more abundant in
345 adipose tissue from PDAC mice. We performed immunohistochemical staining of HuR in
346 formalin-fixed, paraffin-embedded sham and PDAC gWAT, iWAT, pancreas, and muscle
347 tissue. HuR staining was significantly increased in the pancreas, gWAT, and iWAT of PDAC
348 mice versus sham controls (**Figure 6B-D, S7-8).** We also observed increased HuR protein
349 abundance by western blotting whole gWAT tissue (**Figure 6E, S4**).

350 **HuR inhibition improves adipose anabolism after fasting in PDAC mice**

351 Since HuR has been established to drive pro-survival pathways in PDAC, we next
352 wanted to determine if preventing HuR binding to target mRNAs could reverse adipose wasting
353 in PDAC cachexia [26]. To do this, we treated PDAC mice with a selective HuR inhibitor, KH-3,

354 which prevents binding of HuR to its target mRNA sequence [33]. All mice received orthotopic
355 PDAC tumor injections and were fed *ad libitum* then fasted 24h with or without a 24h refeed at
356 mid-cachexia (9 days after injection). In each feeding group, mice were treated with the HuR
357 inhibitor KH-3 (100 mg/kg) or vehicle at 6-, 8-, and 10-days post-injection. Cumulative food
358 intake between vehicle and KH-3 groups was not statistically significant prior to fast. KH-3
359 treated PDAC mice gained significantly more weight during refeeding compared to vehicle-
360 treated mice (**Figure 7A-B**). Refeeding was associated with larger tumors in both vehicle and
361 KH-3 groups, likely due to both log growth and the propensity for mice to become dehydrated
362 during fasting (**Figure 7C**). KH-3 treatment itself had no effect on tumor growth over this time
363 interval. In the presence of KH-3, refeeding increased WAT mass of PDAC animals, which was
364 not observed in vehicle-treated PDAC mice (**Figure 7D-F**). These data indicate that mice
365 treated with KH-3 shows signs of functional anabolism that are lacking in PDAC mice given
366 vehicle treatment. This effect is evident despite the fact that KH-3 treated mice tended to lose
367 more WAT mass during fasting than vehicle-treated mice. Pro-anabolic effects of KH-3 are
368 specific to adipose tissue, as gastrocnemius muscle mass was not changed between
369 fast/refeed, or vehicle/KH-3 treatment (**Figure 7F**). KH-3 treatment did not restore expression
370 of adipogenic (*Cebpa, Adipoq, Lep*, *Retn*) or lipogenic (*Fasn, Dgat1, Dgat2, Nr1h3, Scd1,*
371 *Srebp1c*) genes (**Figure 8B-C, E-F**). HuR inhibition also did not impact lipolysis gene
372 expression (*Atgl* and *Lipe*) (**Figure 8A, D**). Thus, we show a role for HuR in adipose tissue
373 metabolism during PDAC-associated cachexia, whereby inhibiting HuR improved anabolism
374 and adipose retention, although without restoring the expression of genes associated with
375 adipogenesis and lipogenesis.

376 **DISCUSSION**

377 This work evaluates the relative contributions of enhanced catabolism and impaired
378 anabolism on fat wasting by investigating adipose tissue response to different nutritional
379 contexts and HuR inhibition in cachectic mice. We demonstrate that our murine model of
380 PDAC cachexia exhibits a near-complete deficit in adipose tissue anabolism in the context of
381 reduced lipolysis. We further identify HuR as a potential molecular mediator of adipogenesis
382 during pancreatic cancer progression. In cultured adipocytes, we showed that PDAC
383 conditioned media does not induce a strong lipolytic response. Although the sensitivity of the
384 glycerol release assay was limited by the absence of BSA as a free fatty acid acceptor,
385 lipolysis and lipogenesis protein and mRNA expression data were congruent with later findings
386 in vivo. Altogether, this emphasizes that PDAC-derived factors are sufficient to impair adipose
387 anabolism, which corroborates a growing body of literature that challenges the dogma that fat
388 wasting occurs as a result of only enhanced catabolism [16-18].
389 Our study implicates the RNA-binding protein HuR in the inhibition of adipogenesis and
390 lipogenesis in adipose tissue. HuR can impact the transcriptome through both RNA binding
391 and HuR-dependent splicing [26]. One documented mechanism of HuR-mediated
392 adipogenesis regulation is via HuR binding to adipogenesis upstream regulator *Pparg*, which
393 suppresses *Adipoq* protein expression in a non-transcriptionally dependent manner [34]. In our
394 RNA sequencing, we did not observe increased HuR expression, although others reported
395 increased HuR expression in response to nuclear factor-kappa B (NF-κB) signaling [35].
396 Alternatively, we identified HuR as an upstream regulator based on adipose transcriptomic
397 changes associated with PDAC. In this context, HuR is more likely controlled post-
398 transcriptionally, although further investigation is needed to identify the specific PDAC-
399 associated factors that may activate HuR stability and nuclear translocation [36].

400 Small molecule antagonists of HuR, such as KH-3, are currently in development and
401 have been found to have anti-tumor effects [26, 37]. In our studies, KH-3 restored adipose
402 anabolism but also induced severe hemolytic anemia in all treated mice (**Figure S9**). Tumor
403 size was not impacted by KH-3 treatment, likely because of the short period of dosing.
404 However, studies aimed to evaluate tumor growth over 5 weeks documented slower tumor
405 growth and fewer metastases in KH-3-treated mice [38]. KH-3 did not reverse the
406 transcriptional repression of adipogenesis and lipogenesis observed in WAT from PDAC mice.
407 If KH-3 restores adipogenesis by blocking HuR binding to RNA, we interpret these data to
408 suggest that HuR acts post-transcriptionally to suppress adipose anabolism, although we
409 cannot rule out non-HuR-mediated (i.e., off-target) mechanisms of action. In our studies, the
410 anti-cachectic effects of KH-3 were specific to adipose tissue and did not preserve skeletal
411 muscle mass. Although prior studies link muscle and adipose wasting, these models are all
412 characterized by enhanced lipolysis and browning [30]. As evidenced by the adipose-specific
413 benefits of KH-3 with concurrent muscle wasting, in our model, adipose and muscle wasting
414 appear to be driven by independent mechanisms. Continued improvement of HuR antagonists
415 could lead to therapeutics that restore anabolic potential in adipose tissue, providing a novel
416 approach to alleviating one symptom of cachexia, while also providing anti-tumor benefits.
417 In addition to impaired anabolic potential in adipose tissue, our PDAC model also
418 presents suppressed lipolysis. Suppressed lipolysis could contribute to systemic defects in
419 energy utilization in cancer cachexia. Prior work from our group shows that PDAC impairs
420 hepatic lipid oxidation but that this does not result in lipid accumulation or fatty liver [32]. It is
421 possible that impaired lipolysis contributes to global metabolic disruption by limiting circulating
422 lipid substrates relative to the degree of caloric deficit. Further interrogation is needed to

423 understand how improved fat retention through HuR inhibition might impact lipid mobilization
424 and systemic metabolism.

425 Our work identifies impaired adipose anabolism and increased HuR signaling as unique
426 components of adipose wasting in cachexia. Although much of the focus in cachexia research
427 and treatment is on skeletal muscle, multiple recent reports demonstrate that adipose loss in
428 PDAC cachexia is a poor prognostic indicator, independent of muscle loss [5, S9-10]. This
429 further supports existing work describing heterogeneity within cancer cachexia patients [39].
430 Moving forward, accounting for cachexia patient heterogeneity, including adipose wasting and
431 loss of anabolic adipose potential, in clinical trial design may lead to increased therapeutic
432 success. The work presented here provides a strong foundation for continuing to evaluate
433 therapeutics designed to improve adipogenesis and lipogenesis in the context of PDAC
434 cachexia.

435 **ACKNOWLEDGEMENTS**

436 We thank all members of the Aaron Grossberg and Jonathan Brody labs for their helpful
437 discussion and suggestions. We also would like to thank Dr. Laing Xu (Department of
438 Molecular Biosciences, University of Kansas, Lawrence, Kansas) for generously providing us
439 with the KH-3 compound. Author contributions are: Conceptualization, KP, AJG. Methodology,
440 KP, HM, PP, GM, AC, AJG. Validation, PCAW, KP, HM, BW, PP. Formal Analysis, PCAW, KP,
441 HM, BW, PP, GM, AC, AJG. Investigation, PCAW, KP, HM, BW, PP, GM, AC. Writing—
442 Original Draft, PCAW, BLW. Writing – Review and Editing, PCAW, PP, JB, AJG. Visualization,
443 PCAW, KP, HM, BW, PP, GM, AC. Supervision, JB, AJG. Project Administration, JB, AJG.
444 Funding Acquisition, JB, AJG. All authors approved this manuscript.

Funding: This work was supported by National Cancer Institute grants K99CA286709 (PCAW), R37CA280692 (AJG), R01264133 (AJG), and K08245188 AJG), R01 CA212600 (JRB), U01CA224012-03 (JRB), R21 CA263996 (JRB), AACR Grant-15-90-25-BROD (JRB), the Hirshberg Foundation (JRB), and support from the Brenden Colson Center for Pancreatic Care (AJG, JRB, and PCAW). This work is also supported by the Histopathology Shared Resource for pathology studies (University Shared Resource Program at Oregon Health and Sciences University and the Knight Cancer Institute (P30 CA069533 and P30 CA069533 13S5)). The research reported in this publication used computational infrastructure supported by the Office of Research Infrastructure Programs, Office of the Director, of the National Institutes of Health (S10OD034224). The content is solely the responsibility of the authors and does not necessarily represent the official views of the National Institutes of Health.

Conflict of interest: The authors do not declare any conflicts of interest.

Ethical standards: The authors of this manuscript certify that they comply with the ethical guidelines for authorship and publishing in the Journal of Cachexia, Sarcopenia and Muscle. [40] All human and animal studies were approved by the appropriate ethics committees and were therefore performed in accordance with the ethical standards laid down in the 1964 Declaration of Helsinki and its later amendments. All human subjects provided informed consent and any identifying information of individual patients has been omitted.

464 **FIGURE LEGENDS**

465 **Figure 1: Adipocytes suppress lipogenesis in response to pancreatic ductal**
466 **adenocarcinoma-conditioned media. (A**) Representative brightfield images of differentiated
467 3T3-L1 cells treated with control media (top) or KPC CM (bottom) for **6** days. Scale bars
468 represent 70 um. **(B)** Quantification of Oil Red O staining. N = 4 wells per condition. (**C-E**) 3T3-
469 L1 cells were fully differentiated and then treated with control, KPC-conditioned, or
470 isoproterenol (10 uM) media for 1, 3, and 24 hours in the absence of FBS and insulin. N = 3
471 wells per timepoint/condition. (**C**) Media glycerol levels, normalized by hours of collection .
472 Conditioned media and control media alone did not contain glycerol above background (assay
473 buffer only) levels. (**D**) Serine 563 phosphorylated HSL protein levels normalized to total HSL
474 protein levels. (**E**) Serine 660 phosphorylated HSL protein levels normalized to total HSL
475 protein levels. (**F**) mRNA expression of lipolysis and lipogenesis genes. N= 3 wells per
476 condition, normalized to 18S expression. Panels B and F tested with t-test. Panels C-E tested
477 with two-way ANOVA with Tukey correction for multiple comparisons. $p<0.05$, $^{**}p<0.01$,
478 $^{***}p<0.001$, and $^{****}p<0.0001$.
479
480 **Figure 2: Pancreatic ductal adenocarcinoma is associated with decreased fat pad mass**
481 ***in vivo***. (**A-E**)Wildtype C57BL/6J mice with PDAC or sham implantations were fed *ad libitum*
482 or fasted 16 h at mid-cachexia (9 days after injection). Animals were euthanized 10 or 11 days
483 after tumor implantation following a 16 h fast. N=5 sham, 6 PDAC male mice per feeding
484 condition. **(A)** Daily body mass. Statistically tested with 3-way ANOVA $p<0.0001$ for time, time
485 x fast; $p=0.0073$ for fast; $p=0.0097$ for time x tumor status; $p=0.0167$ for tumor status. (**B**)
486 Cumulative food intake. Statistically tested with 3-way ANOVA $p<0.0001$ for time, time x fast;
487 $p=0.0035$ for time x tumor status. (**C**) Terminal pancreas/tumor mass. (**D-E**) Body composition
488 changes in total adiposity were characterized from baseline (pre-tumor implantation) to pre-fast
489 between sham and PDAC mice (**C**), and from pre- to post-fast (**D**). (**F**) Terminal gWAT and
490 iWAT mass following 24 h fast 14 days after injection. N=5 male mice per *ad lib* group, 5 male
491 mice sham fast, 3 male mice PDAC fast. 2x2 analyses were statistically tested with two-way
492 ANOVA or mixed effects model with Tukey multiple comparisons. $^{*}p<0.05$, $^{**}p<0.01$, and
493 $^{****}p<0.0001$.
494
495 **Figure 3: Pancreatic ductal adenocarcinoma impairs lipolysis and adipogenesis *in vivo*.**
496 **(A)** Measurement of lipolysis (glycerol release) in explants derived from gWAT collected 10
497 days after tumor implantation. Lipolysis was induced by the β-adrenergic agonist isoproterenol
498 (10 μM). N=6 male mice per group. Statistically tested with two-way ANOVA with uncorrected
499 Fisher's LSD test to compare groups. (**D**) mRNA levels of lipolysis and browning genes in
500 gWAT collected 10 days post-implantation from 24 h-fasted and *ad libitum*-fed mice,
501 normalized to 18S expression. N=5 male mice sham/fasted; 3 male, 3 female mice sham/ad
502 lib; 6 male mice PDAC/fasted; 3 male, 2 female mice PDAC/ad lib. (**E**) mRNA expression of
503 lipolysis and browning genes in iWAT collected 11 days post-implantation from *ad libitum*-fed
504 mice, normalized to beta actin expression. N=4 male mice per group. (**F**) Western blot
505 analysis of PDAC and Sham gWAT protein for HSL (83 kDa) and ATGL (55 kDa) (left) and
506 Serine 563- and Serine 660-phosphorylated HSL protein levels normalized to total HSL protein
507 levels (right). N=5 male mice per group. Protein normalized to vinculin (124 kDa). 2x2 data

were statistically tested with two-way ANOVA with Tukey multiple comparisons comparing tumor experimental groups to sham controls. Pairwise comparisons were made with unpaired t-test. *p<0.05, **p<0.01, ***p<0.001, and ****p<0.0001.

Figure 4: PDAC downregulates pathways associated with adipogenesis. RNAseq on gWAT from *ad libitum*-fed PDAC and sham mice collected 14 days post tumor implantation. N=2 female, 3 male PDAC; 3 female, 2 male sham. **(A)** Volcano plot of differentially expressed genes in gWAT. Blue dots represent significantly downregulated genes (log_2 fold change < -1 and adj p<0.05). while red dots represent significantly upregulated genes (log_2 fold change >1 and adj p<0.05). Grey dots are insignificant. Labels denote significant differentially expressed genes from the Hallmark Adipogenesis pathway. **(B)** Broad Institute GSEA showing significantly enriched pathways in PDAC gWAT relative to sham gWAT (pathway p<0.05). Blue is decreased expression, red is increased expression. **(C)** Heat map of Hallmark Adipogenesis pathways constituents in PDAC and Sham gWAT. Scale represents row-normalized raw counts. **(D)** qPCR validation of adipogenesis and lipogenesis genes in in gWAT collected 10 days post-implantation from 24 h-fasted and *ad libitum*-fed mice. N=5 male mice sham/fasted; 3 male, 3 female mice sham/ad lib; 6 male mice PDAC/fasted; 3 male, 2 female mice PDAC/ad lib. Statistically tested with two-way ANOVA with Tukey multiple comparisons comparing tumor experimental groups to sham controls. **(E)** qPCR validation of adipogenesis and lipogenesis genes in iWAT from ad lib fed mice collected 11 days post implantation. N=4 male mice per group. Statistically tested with unpaired t-test. *p<0.05, **p<0.01, ***p<0.001, and ****p<0.0001.

Figure 5: Adipose tissue anabolism is impaired in orthotopic PDAC mice after refeeding. Wildtype C57BL/6J mice with PDAC were fed *ad libitum* for 9 days then fasted 24 h with or without a 24 h refeeding period. Sham mice were pair-fed daily to the average food intake of the PDAC group from 2 days post-implantation until study end. Animals were euthanized 10 or 11 days after tumor implantation following the 24 h fast (10 d) or 24 h refeed (11 d). N=3 male and 3 female mice per group. **(A)** Cumulative food intake. Statistically tested with 3-way ANOVA. P<0.0001 for time, p=0.0344 for time x tumor status. **(B)** Daily body mass. Statistically tested with 3-way ANOVA. P<0.0001 for time, p=0.002 for time x tumor status. iWAT (**C**) and gWAT (**D**) mass normalized to initial body mass. mRNA expression of anabolic genes in gWAT (**E**) and iWAT (**F**), normalized to beta actin expression. Data represented in C-F were statistically tested with two-way ANOVA with Tukey multiple comparisons comparing PDAC groups to sham controls. *p<0.05, and ****p<0.0001.

Figure 6: HuR is highly expressed in PDAC orthotopic pancreas and fat tissue. (A) Selected upstream regulator predictions from Ingenuity Pathway Analysis of differentially expressed genes in gWAT. **(B-D)** Representative images and quantification of immunohistochemical detection of HuR in tissue from PDAC and sham mice. **(B)** Pancreas N=4 male and 4 female mice per group. **(C)** gWAT N=4 male and 4 female mice per group. **(D)** iWAT N=3 female, 2 male sham and 2 female, 3 male PDAC. (**E**) Western blot analysis of PDAC and Sham gWAT protein for HuR. N=5 male mice per group. HuR protein (36 kDa)

551 normalized to vinculin protein (124 kDa). Scale bars represent 100 um. Statistically tested with
552 t-test. *p<0.05, **p<0.01, ***p<0.001, and ****p<0.0001.
553
554 **Figure 7: HuR inhibition improves adipose anabolism after fasting in PDAC mice**.
555 Wildtype C57BL/6J mice with PDAC were fed *ad libitum* for 9 days then fasted 24 h with or
556 without a 24 h refeed. In each feeding paradigm, groups were treated with either vehicle or the
557 HuR antagonist, KH-3, then euthanized 10 or 11 days after tumor implantation following the 24
558 h fast or 24 h refeed. Vehicle-treated mice were pair-fed to the KH-3 treated group's average
559 food intake from 8 days post-implantation until study end. N=7 male mice per group. **(A)**
560 Cumulative food intake, statistically tested as an unpaired t-test of vehicle vs KH-3 treatment at
561 day 9 (prior to fast) p =0.1121. **(B)** Change in body weight after refeeding, statistically tested
562 with unpaired t-test. **(C)** Terminal pancreas mass. **(D)** Terminal gWAT mass. **(E)** Terminal
563 iWAT mass. **(F)** Terminal gastrocnemius mass. 2x2 analyses were statistically tested with two-
564 way ANOVA with Tukey multiple comparisons*p<0.05, and **p<0.01.
565
566 **Figure 8: HuR inhibition does not improve gene expression patterns associated with**
567 **anabolism**. mRNA levels of lipolysis **(A),** adipogenesis **(B),** and lipogenesis **(C)** genes in
568 gWAT, normalized to beta actin expression. mRNA levels of lipolysis **(D),** adipogenesis **(E),**
569 and lipogenesis **(F)** genes in iWAT, normalized to beta actin expression. Data were statistically
570 tested with two-way ANOVA with Tukey multiple comparisons correction. N=7 male mice per
571 group. *p<0.05, **p<0.01, ***p<0.001, and ****p<0.0001.
572

573

574

575 **REFERENCES**

576 1. Baracos VE, Martin L, Korc M, Guttridge DC, Fearon KCH. Cancer-associated
577 cachexia. Nat Rev Dis Primers. 2018;4:17105. doi:10.1038/nrdp.2017.105
578 2. von Haehling S, Anker MS, Anker SD. Prevalence and clinical impact of cachexia in
579 chronic illness in Europe, USA, and Japan: facts and numbers update 2016. J Cachexia
580 Sarcopenia Muscle. 2016;7:507-9. doi:10.1002/jcsm.12167
581 3. Fearon K, Strasser F, Anker SD, Bosaeus I, Bruera E, Fainsinger RL, et al. Definition
582 and classification of cancer cachexia: an international consensus. Lancet Oncol. 2011;12:489-
583 95. doi:10.1016/S1470-2045(10)70218-7
584 4. Fearon K, Arends J, Baracos V. Understanding the mechanisms and treatment options
585 in cancer cachexia. Nat Rev Clin Oncol. 2013;10:90-9. doi:10.1038/nrclinonc.2012.209
586 5. Kays JK, Shahda S, Stanley M, Bell TM, O'Neill BH, Kohli MD, et al. Three cachexia
587 phenotypes and the impact of fat-only loss on survival in FOLFIRINOX therapy for pancreatic
588 cancer. Journal of cachexia, sarcopenia and muscle. 2018;9:673-84.
589 6. Mantovani G, Maccio A, Lai P, Massa E, Ghiani M, Santona MC. Cytokine activity in
590 cancer-related anorexia/cachexia: role of megestrol acetate and medroxyprogesterone
591 acetate. Semin Oncol. 1998;25:45-52.
592 7. Straub RH, Cutolo M, Buttgereit F, Pongratz G. Energy regulation and neuroendocrine-
593 immune control in chronic inflammatory diseases. J Intern Med. 2010;267:543-60.
594 doi:10.1111/j.1365-2796.2010.02218.x
595 8. Argiles JM, Busquets S, Toledo M, Lopez-Soriano FJ. The role of cytokines in cancer
596 cachexia. Curr Opin Support Palliat Care. 2009;3:263-8. doi:10.1097/SPC.0b013e3283311d09

597 9. MacDonald N, Easson AM, Mazurak VC, Dunn GP, Baracos VE. Understanding and
598 managing cancer cachexia. J Am Coll Surg. 2003;197:143-61. doi:10.1016/S1072-
599 7515(03)00382-X
600 10. Carson JL, Hernandez M, Jaspers I, Mills K, Brighton L, Zhou H, et al. Interleukin-13
601 stimulates production of nitric oxide in cultured human nasal epithelium. In Vitro Cell Dev Biol
602 Anim. 2018;54:200-4. doi:10.1007/s11626-018-0233-y
603 11. Haslett PA. Anticytokine approaches to the treatment of anorexia and cachexia. Semin
604 Oncol. 1998;25:53-7.
605 12. Moldawer LL, Copeland EM, 3rd. Proinflammatory cytokines, nutritional support, and
606 the cachexia syndrome: interactions and therapeutic options. Cancer. 1997;79:1828-39.
607 13. Das SK, Eder S, Schauer S, Diwoky C, Temmel H, Guertl B, et al. Adipose triglyceride
608 lipase contributes to cancer-associated cachexia. Science. 2011;333:233-8.
609 14. Petruzzelli M, Schweiger M, Schreiber R, Campos-Olivas R, Tsoli M, Allen J, et al. A
610 switch from white to brown fat increases energy expenditure in cancer-associated cachexia.
611 Cell metabolism. 2014;20:433-47.
612 15. Taylor J, Uhl L, Moll I, Hasan SS, Wiedmann L, Morgenstern J, et al. Endothelial Notch1
613 signaling in white adipose tissue promotes cancer cachexia. Nature Cancer. 2023;4:1544-60.
614 16. Langer HT, Ramsamooj S, Dantas E, Murthy A, Ahmed M, Ahmed T, et al. Restoring
615 adiponectin via rosiglitazone ameliorates tissue wasting in mice with lung cancer. Acta
616 Physiologica. 2024;e14167.
617 17. Jang HJ, Kim HY, Lyu JH, Muthamil S, Shin UC, Kim HS, et al. Bee (Apis mellifera L.
618 1758) wax restores adipogenesis and lipid accumulation of 3T3-L1 cells in cancer-associated
619 cachexia condition. Food Science & Nutrition. 2024;

620 18. Tien S-C, Chang C-C, Huang C-H, Peng H-Y, Chang Y-T, Chang M-C, et al. Exosomal
621 miRNA 16-5p/29a-3p from pancreatic cancer induce adipose atrophy by inhibiting
622 adipogenesis and promoting lipolysis. Iscience. 2024;27:
623 19. Cook KB, Kazan H, Zuberi K, Morris Q, Hughes TR. RBPDB: a database of RNA-
624 binding specificities. Nucleic Acids Res. 2011;39:D301-8. doi:10.1093/nar/gkq1069
625 20. Gerstberger S, Hafner M, Tuschl T. A census of human RNA-binding proteins. Nat Rev
626 Genet. 2014;15:829-45. doi:10.1038/nrg3813
627 21. Pihlajamaki J, Lerin C, Itkonen P, Boes T, Floss T, Schroeder J, et al. Expression of the
628 splicing factor gene SFRS10 is reduced in human obesity and contributes to enhanced
629 lipogenesis. Cell Metab. 2011;14:208-18. doi:10.1016/j.cmet.2011.06.007
630 22. Brosch M, von Schonfels W, Ahrens M, Nothnagel M, Krawczak M, Laudes M, et al.
631 SFRS10--a splicing factor gene reduced in human obesity? Cell Metab. 2012;15:265-6; author
632 reply 7-9. doi:10.1016/j.cmet.2012.02.002
633 23. Huot ME, Vogel G, Zabarauskas A, Ngo CT, Coulombe-Huntington J, Majewski J, et al.
634 The Sam68 STAR RNA-binding protein regulates mTOR alternative splicing during
635 adipogenesis. Mol Cell. 2012;46:187-99. doi:10.1016/j.molcel.2012.02.007
636 24. Chou CF, Lin YY, Wang HK, Zhu X, Giovarelli M, Briata P, et al. KSRP ablation
637 enhances brown fat gene program in white adipose tissue through reduced miR-150
638 expression. Diabetes. 2014;63:2949-61. doi:10.2337/db13-1901
639 25. Dai N, Zhao L, Wrighting D, Kramer D, Majithia A, Wang Y, et al. IGF2BP2/IMP2-
640 Deficient mice resist obesity through enhanced translation of Ucp1 mRNA and Other mRNAs
641 encoding mitochondrial proteins. Cell Metab. 2015;21:609-21. doi:10.1016/j.cmet.2015.03.006

642 26. Finan JM, Sutton TL, Dixon DA, Brody JR. Targeting the RNA-binding protein HuR in
643 cancer. Cancer Research. 2023;83:3507-16.
644 27. Siang DTC, Lim YC, Kyaw AMM, Win KN, Chia SY, Degirmenci U, et al. The RNA-
645 binding protein HuR is a negative regulator in adipogenesis. Nat Commun. 2020;11:213.
646 doi:10.1038/s41467-019-14001-8
647 28. Michaelis KA, Zhu X, Burfeind KG, Krasnow SM, Levasseur PR, Morgan TK, et al.
648 Establishment and characterization of a novel murine model of pancreatic cancer cachexia. J
649 Cachexia Sarcopenia Muscle. 2017;8:824-38. doi:10.1002/jcsm.12225
650 29. Schweiger M, Eichmann TO, Taschler U, Zimmermann R, Zechner R, Lass A.
651 Measurement of lipolysis. In: Elsevier; 2014. pp. 171-93.
652 30. Rupert JE, Narasimhan A, Jengelley DH, Jiang Y, Liu J, Au E, et al. Tumor-derived IL-6
653 and trans-signaling among tumor, fat, and muscle mediate pancreatic cancer cachexia.
654 Journal of Experimental Medicine. 2021;218:e20190450.
655 31. Liberzon A, Birger C, Thorvaldsdóttir H, Ghandi M, Mesirov JP, Tamayo P. The
656 molecular signatures database hallmark gene set collection. Cell systems. 2015;1:417-25.
657 32. Arneson-Wissink PC, Mendez H, Pelz K, Dickie J, Bartlett AQ, Worley BL, et al. Hepatic
658 signal transducer and activator of transcription-3 signalling drives early-stage pancreatic
659 cancer cachexia via suppressed ketogenesis. J Cachexia Sarcopenia Muscle. 2024;15:975-88.
660 doi:10.1002/jcsm.13466
661 33. Wu X, Gardashova G, Lan L, Han S, Zhong C, Marquez RT, et al. Targeting the
662 interaction between RNA-binding protein HuR and FOXQ1 suppresses breast cancer invasion
663 and metastasis. Commun Biol. 2020;3:193. doi:10.1038/s42003-020-0933-1

664 34. Hwang JS, Lee WJ, Hur J, Lee HG, Kim E, Lee GH, et al. Rosiglitazone-dependent
665 dissociation of HuR from PPAR-γ regulates adiponectin expression at the posttranscriptional
666 level. The FASEB Journal. 2019;33:7707-20. doi:10.1096/fj.201802643r
667 35. Kang MJ, Ryu BK, Lee MG, Han J, Lee JH, Ha TK, et al. NF-κB Activates
668 Transcription of the RNA-Binding Factor HuR, via PI3K-AKT Signaling, to Promote Gastric
669 Tumorigenesis. Gastroenterology. 2008;135:2030-42.e3. doi:10.1053/j.gastro.2008.08.009
670 36. Grammatikakis I, Abdelmohsen K, Gorospe M. Posttranslational control of HuR
671 function. Wiley Interdisciplinary Reviews: RNA. 2017;8:e1372.
672 37. Huang Z, Liu S, Tang A, Wu X, Aube J, Xu L, et al. Targeting RNA-binding protein HuR
673 to inhibit the progression of renal tubular fibrosis. Journal of Translational Medicine.
674 2023;21:428.
675 38. Dong R, Chen P, Polireddy K, Wu X, Wang T, Ramesh R, et al. An RNA-Binding
676 Protein, Hu-antigen R, in Pancreatic Cancer Epithelial to Mesenchymal Transition, Metastasis,
677 and Cancer Stem Cells. Mol Cancer Ther. 2020;19:2267-77. doi:10.1158/1535-7163.Mct-19-
678 0822
679 39. Fearon Kenneth CH, Glass David J, Guttridge Denis C. Cancer Cachexia: Mediators,
680 Signaling, and Metabolic Pathways. Cell Metabolism. 2012;16:153-66.
681 doi:10.1016/j.cmet.2012.06.011
682 40. von Haehling S, Coats AJ, Anker SD. Ethical guidelines for publishing in the Journal of
683 Cachexia, Sarcopenia and Muscle: update 2021. Wiley Online Library; 2021. pp. 2259-61.

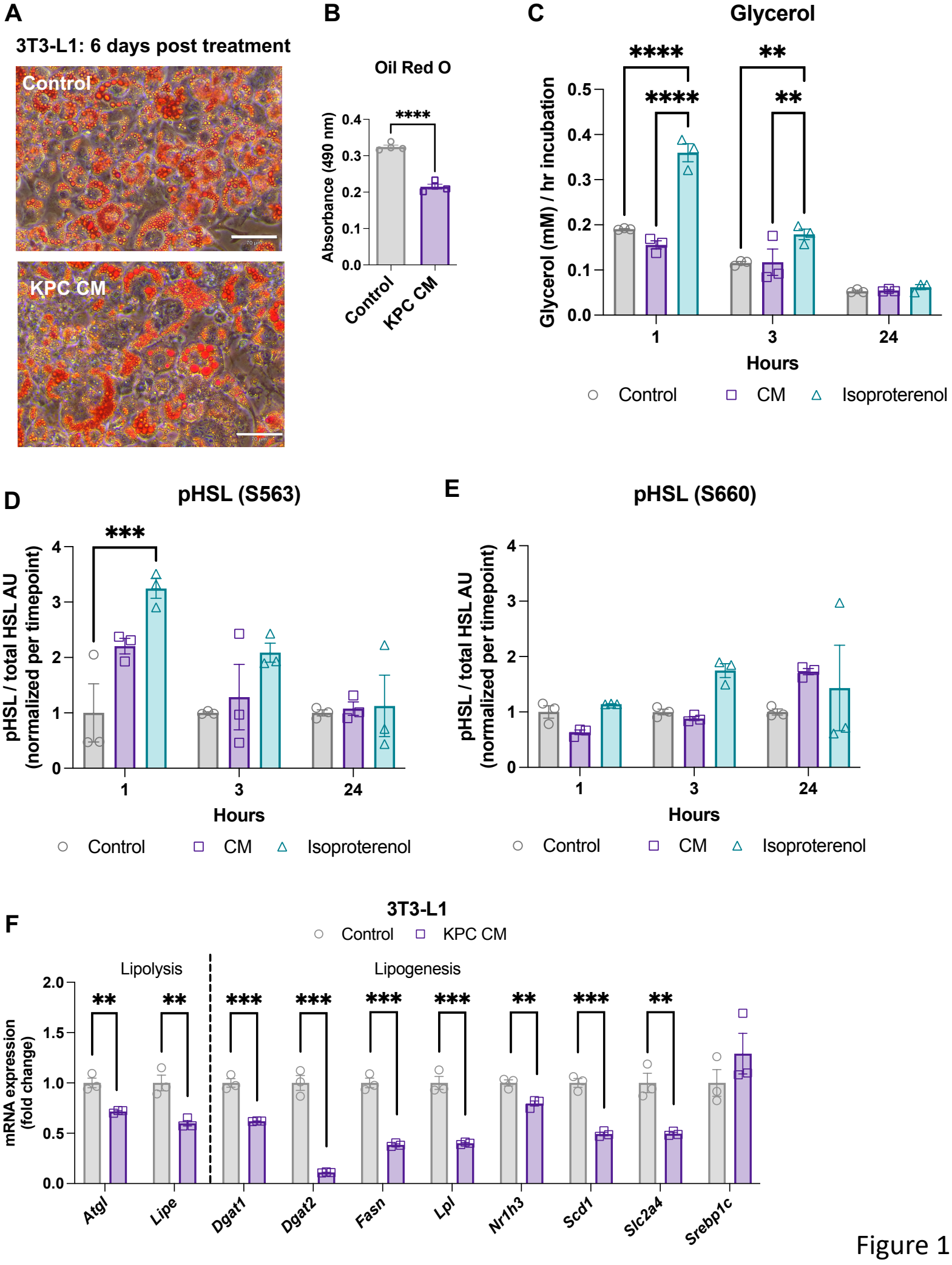
A
3T3-L1: 6 days post treatment
Control
KPC CM
B
Oil Red O
Absorbance (490 nm)
0.0
0.1
0.2
0.3
0.4
****
Control
KPC CM
C
Glycerol
Glycerol (mM) / hr incubation
0.0
0.1
0.2
0.3
0.4
0.5
****
****
**
**
1
3
24
Hours
Control
CM
Isoproterenol
D
pHSL (S563)
pHSL / total HSL AU
(normalized per timepoint)
0
1
2
3
4
***
1
3
24
Hours
Control
CM
Isoproterenol
E
pHSL (S660)
pHSL / total HSL AU
(normalized per timepoint)
0
1
2
3
4
1
3
24
Hours
Control
CM
Isoproterenol
F
3T3-L1
Control
KPC CM
Lipolysis
Lipogenesis
mRNA expression
(fold change)
0.0
0.5
1.0
1.5
2.0
**
**
***
***
***
***
**
***
**
Atgl
Lipe
Dgat1
Dgat2
Fasn
Lpl
Nr1h3
Scd1
Slc2a4
Srebp1c

Figure 1

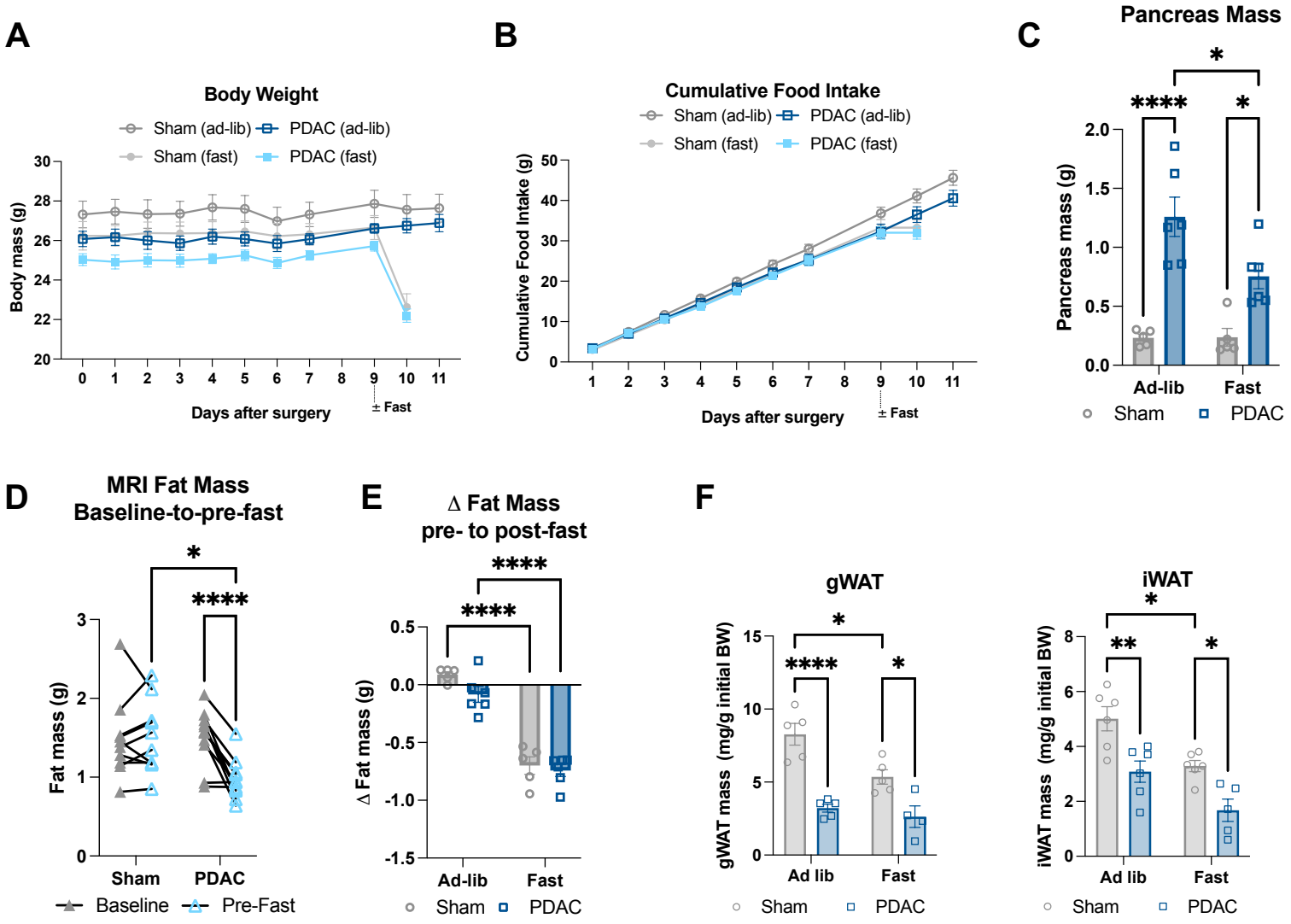
A
Body Weight
Sham (ad-lib)
PDAC (ad-lib)
Sham (fast)
PDAC (fast)
Body mass (g)
Days after surgery
± Fast
B
Cumulative Food Intake
Sham (ad-lib)
PDAC (ad-lib)
Sham (fast)
PDAC (fast)
Cumulative Food Intake (g)
Days after surgery
± Fast
C
Pancreas Mass
Pancreas mass (g)
Ad-lib
Fast
Sham
PDAC
D
MRI Fat Mass
Baseline-to-pre-fast
Fat mass (g)
Sham
PDAC
Baseline
Pre-Fast
E
Δ Fat Mass
pre- to post-fast
Δ Fat mass (g)
Ad-lib
Fast
Sham
PDAC
F
gWAT
gWAT mass (mg/g initial BW)
Ad lib
Fast
Sham
PDAC
iWAT
iWAT mass (mg/g initial BW)
Ad lib
Fast
Sham
PDAC

Figure 2

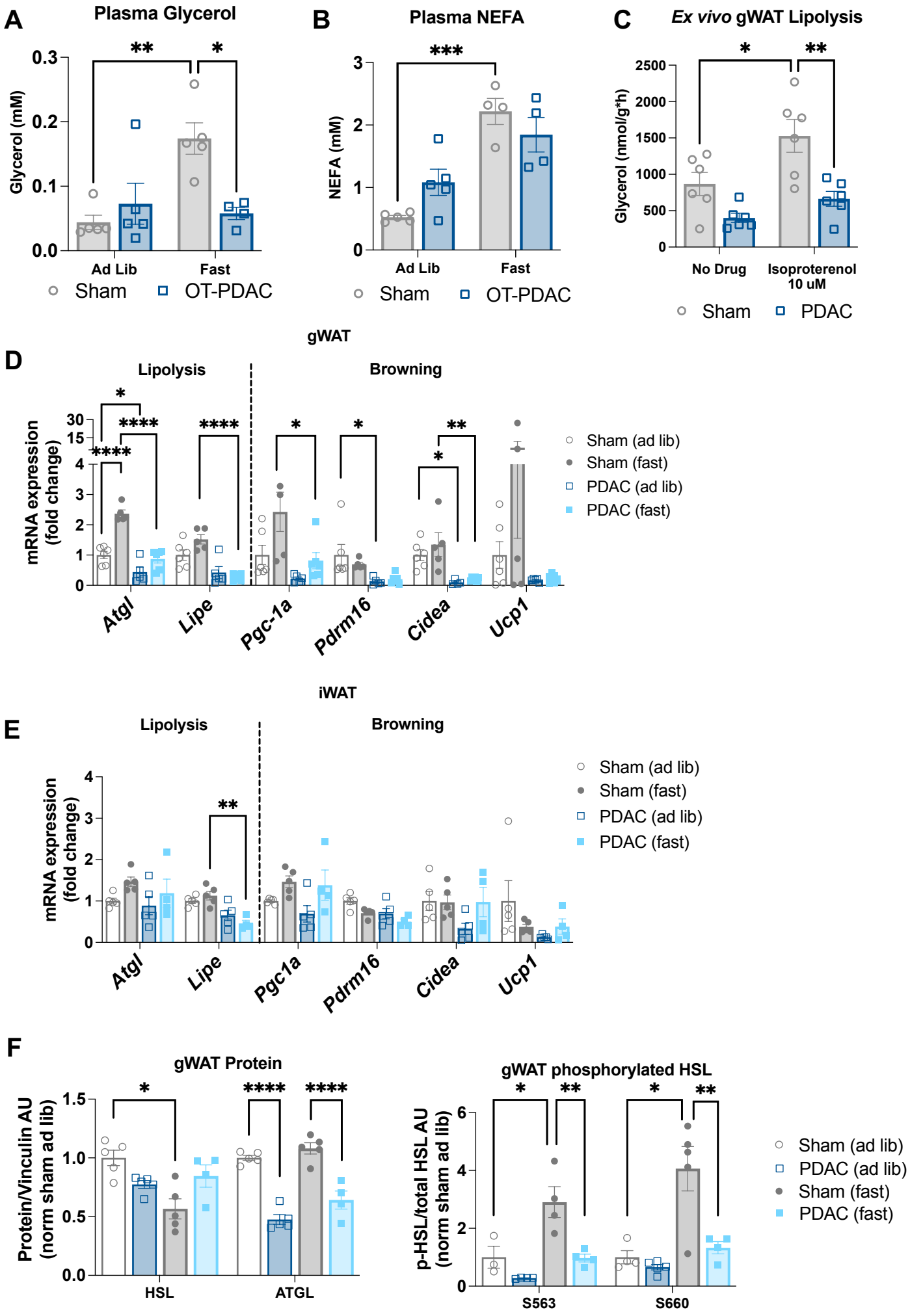
A
Plasma Glycerol
Glycerol (mM)
0.3
0.2
0.1
0.0
**
*
Ad Lib
Fast
Sham
OT-PDAC
B
Plasma NEFA
NEFA (mM)
3
2
1
0
***
Ad Lib
Fast
Sham
OT-PDAC
C
Ex vivo gWAT Lipolysis
Glycerol (nmol/g*h)
2500
2000
1500
1000
500
0
*
**
No Drug
Isoproterenol 10 uM
Sham
PDAC
gWAT
D
Lipolysis
Browning
mRNA expression (fold change)
30
15
4
3
2
1
0
*
****
****
****
*
*
**
*
Atgl
Lipe
Pgc-1a
Pdrm16
Cidea
Ucp1
Sham (ad lib)
Sham (fast)
PDAC (ad lib)
PDAC (fast)
iWAT
E
Lipolysis
Browning
mRNA expression (fold change)
4
3
2
1
0
**
Atgl
Lipe
Pgc1a
Pdrm16
Cidea
Ucp1
Sham (ad lib)
Sham (fast)
PDAC (ad lib)
PDAC (fast)
F
gWAT Protein
Protein/Vinculin AU (norm sham ad lib)
1.5
1.0
0.5
0.0
*
****
****
HSL
ATGL
gWAT phosphorylated HSL
p-HSL/total HSL AU (norm sham ad lib)
6
4
2
0
*
**
*
**
S563
S660
Sham (ad lib)
PDAC (ad lib)
Sham (fast)
PDAC (fast)

Figure 3

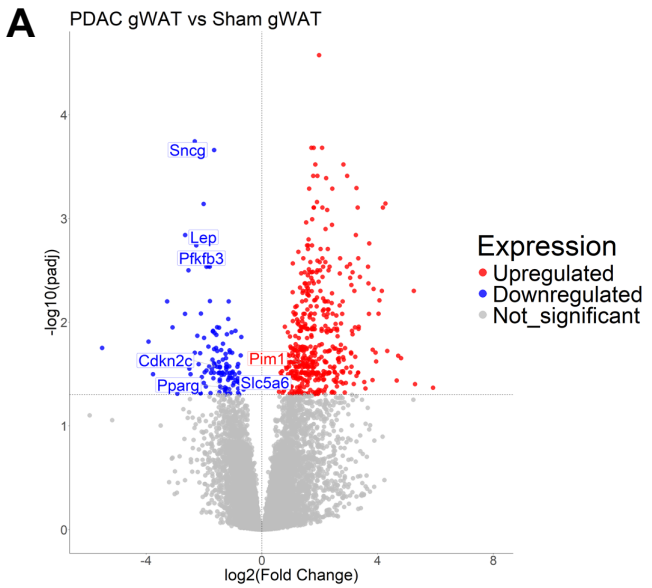
A
PDAC gWAT vs Sham gWAT
Sncg
Lep
Pfkfb3
Cdkn2c
Pparg
Pim1
Slc5a6
Expression
Upregulated
Downregulated
Not_significant
-log10(padj)
log2(Fold Change)

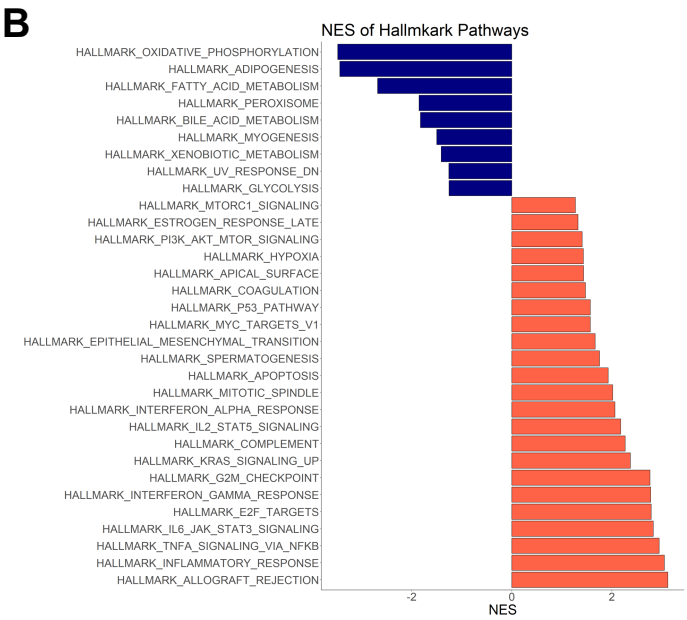
B
NES of Hallmkark Pathways
HALLMARK_OXIDATIVE_PHOSPHORYLATION
HALLMARK_ADIPOGENESIS
HALLMARK_FATTY_ACID_METABOLISM
HALLMARK_PEROXISOME
HALLMARK_BILE_ACID_METABOLISM
HALLMARK_MYOGENESIS
HALLMARK_XENOBIOTIC_METABOLISM
HALLMARK_UV_RESPONSE_DN
HALLMARK_GLYCOLYSIS
HALLMARK_MTORC1_SIGNALING
HALLMARK_ESTROGEN_RESPONSE_LATE
HALLMARK_PI3K_AKT_MTOR_SIGNALING
HALLMARK_HYPOXIA
HALLMARK_APICAL_SURFACE
HALLMARK_COAGULATION
HALLMARK_P53_PATHWAY
HALLMARK_MYC_TARGETS_V1
HALLMARK_EPITHELIAL_MESENCHYMAL_TRANSITION
HALLMARK_SPERMATOGENESIS
HALLMARK_APOPTOSIS
HALLMARK_MITOTIC_SPINDLE
HALLMARK_INTERFERON_ALPHA_RESPONSE
HALLMARK_IL2_STAT5_SIGNALING
HALLMARK_COMPLEMENT
HALLMARK_KRAS_SIGNALING_UP
HALLMARK_G2M_CHECKPOINT
HALLMARK_INTERFERON_GAMMA_RESPONSE
HALLMARK_E2F_TARGETS
HALLMARK_IL6_JAK_STAT3_SIGNALING
HALLMARK_TNFA_SIGNALING_VIA_NFKB
HALLMARK_INFLAMMATORY_RESPONSE
HALLMARK_ALLOGRAFT_REJECTION
NES

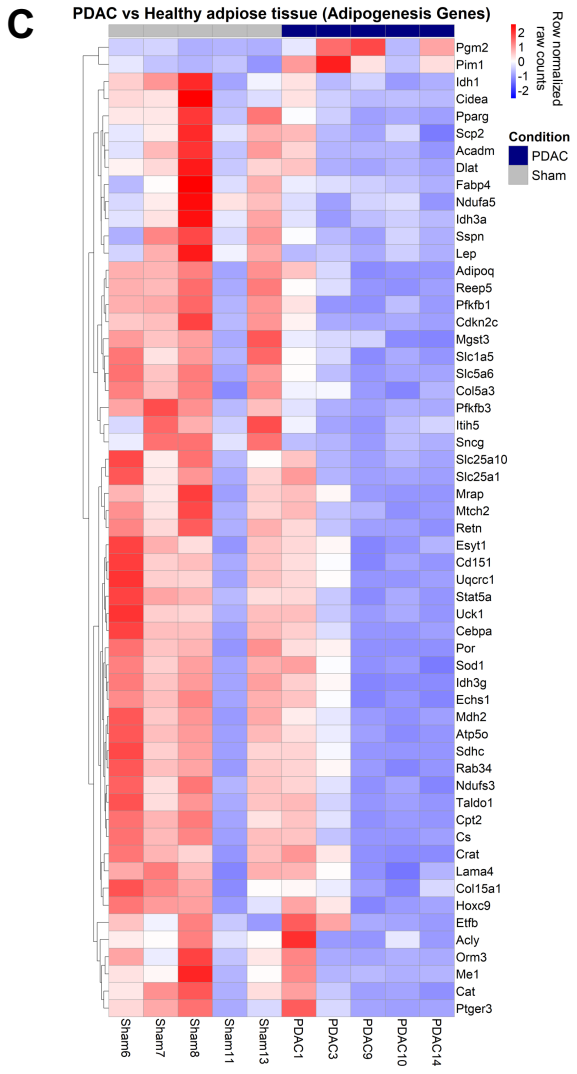
C
PDAC vs Healthy adpiose tissue (Adipogenesis Genes)
Row normalized raw counts
Condition
PDAC
Sham
Pgm2
Pim1
Idh1
Cidea
Pparg
Scp2
Acadm
Dlat
Fabp4
Ndufa5
Idh3a
Sspn
Lep
Adipoq
Reep5
Pfkfb1
Cdkn2c
Mgst3
Slc1a5
Slc5a6
Col5a3
Pfkfb3
Itih5
Sncg
Slc25a10
Slc25a1
Mrap
Mtch2
Retn
Esyt1
Cd151
Uqcrc1
Stat5a
Uck1
Cebpa
Por
Sod1
Idh3g
Echs1
Mdh2
Atp5o
Sdhc
Rab34
Ndufs3
Taldo1
Cpt2
Cs
Crat
Lama4
Col15a1
Hoxc9
Etfb
Acly
Orm3
Me1
Cat
Ptger3
Sham6
Sham7
Sham8
Sham11
Sham13
PDAC1
PDAC3
PDAC9
PDAC10
PDAC14

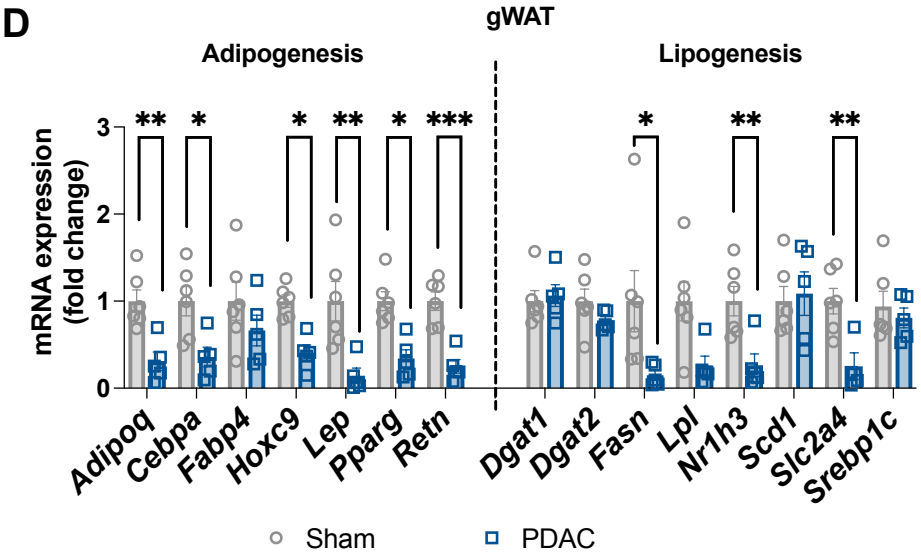
D
gWAT
Adipogenesis
Lipogenesis
mRNA expression (fold change)
Adipoq
Cebpa
Fabp4
Hoxc9
Lep
Pparg
Retn
Dgat1
Dgat2
Fasn
Lpl
Nr1h3
Scd1
Slc2a4
Srebp1c
Sham
PDAC

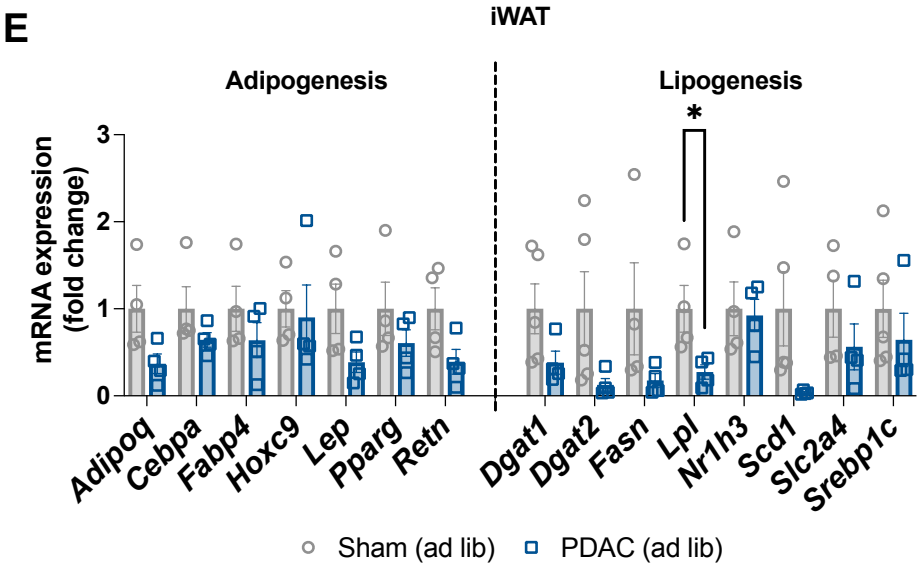
E
iWAT
Adipogenesis
Lipogenesis
mRNA expression (fold change)
Adipoq
Cebpa
Fabp4
Hoxc9
Lep
Pparg
Retn
Dgat1
Dgat2
Fasn
Lpl
Nr1h3
Scd1
Slc2a4
Srebp1c
Sham (ad lib)
PDAC (ad lib)

Figure 4

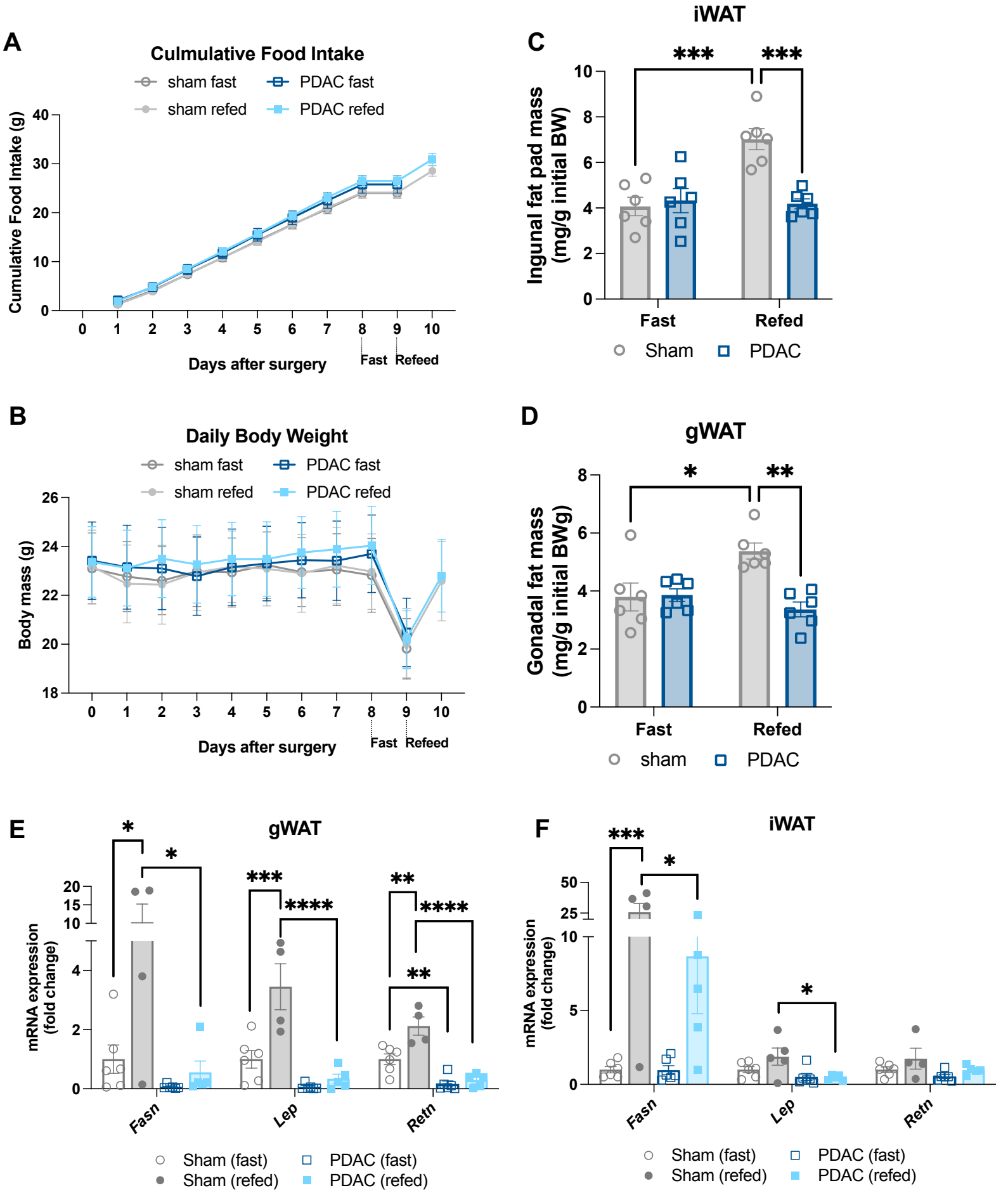
A
Culmulative Food Intake
sham fast
PDAC fast
sham refed
PDAC refed
Cumulative Food Intake (g)
Days after surgery
Fast
Refeed
B
Daily Body Weight
sham fast
PDAC fast
sham refed
PDAC refed
Body mass (g)
Days after surgery
Fast
Refeed
C
iWAT
Ingunal fat pad mass (mg/g initial BW)
Fast
Refed
Sham
PDAC
D
gWAT
Gonadal fat mass (mg/g initial BWg)
Fast
Refed
sham
PDAC
E
gWAT
mRNA expression (fold change)
Fasn
Lep
Retn
Sham (fast)
Sham (refed)
PDAC (fast)
PDAC (refed)
F
iWAT
mRNA expression (fold change)
Fasn
Lep
Retn
Sham (fast)
Sham (refed)
PDAC (fast)
PDAC (refed)

Figure 5

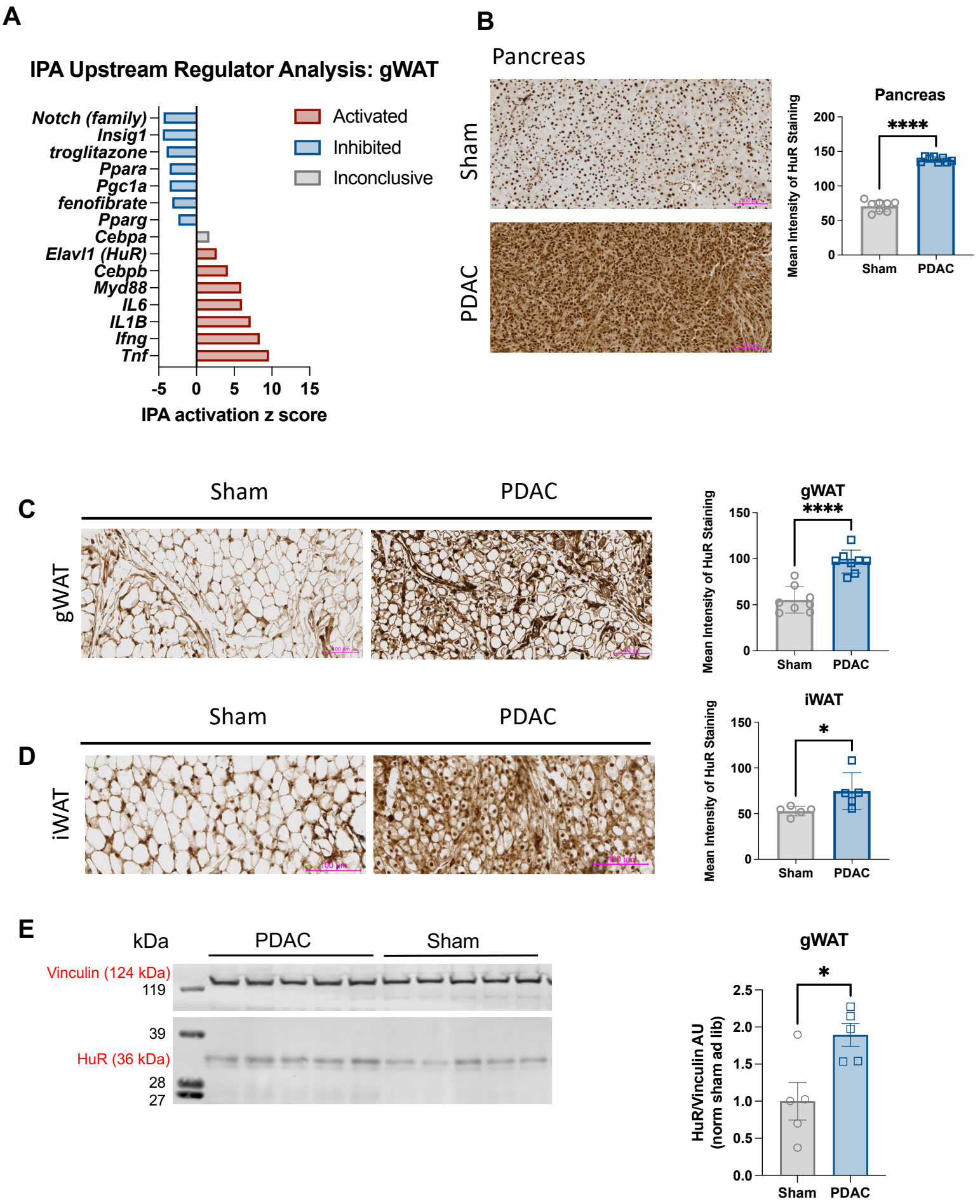
A
IPA Upstream Regulator Analysis: gWAT
Notch (family)
Insig1
troglitazone
Ppara
Pgc1a
fenofibrate
Pparg
Cebpa
Elavl1 (HuR)
Cebpb
Myd88
IL6
IL1B
Ifng
Tnf
Activated
Inhibited
Inconclusive
-5
0
5
10
15
IPA activation z score
B
Pancreas
Sham
PDAC
Pancreas
Mean Intensity of HuR Staining
****
Sham
PDAC
C
Sham
PDAC
gWAT
gWAT
Mean Intensity of HuR Staining
****
Sham
PDAC
D
Sham
PDAC
iWAT
iWAT
Mean Intensity of HuR Staining
*
Sham
PDAC
E
kDa
PDAC
Sham
Vinculin (124 kDa)
119
39
HuR (36 kDa)
28
27
gWAT
*
HuR/Vinculin AU
(norm sham ad lib)
Sham
PDAC

Figure 6

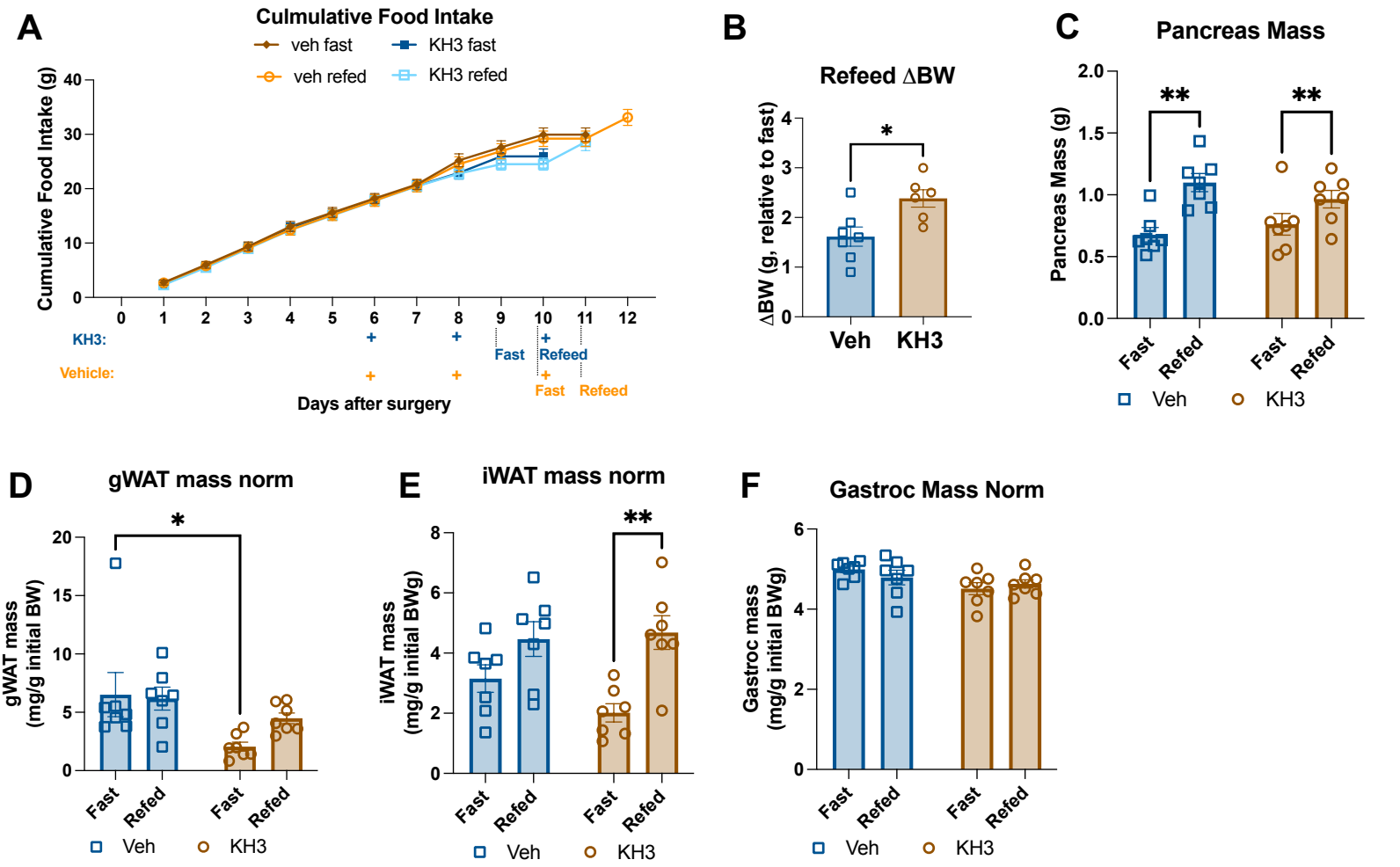
A
Culmulative Food Intake
veh fast
KH3 fast
veh refed
KH3 refed
Cumulative Food Intake (g)
KH3:
Vehicle:
Fast
Refeed
Days after surgery
B
Refeed ΔBW
ΔBW (g, relative to fast)
Veh
KH3
C
Pancreas Mass
Pancreas Mass (g)
Fast
Refed
Veh
KH3
D
gWAT mass norm
gWAT mass (mg/g initial BW)
E
iWAT mass norm
iWAT mass (mg/g initial BWg)
F
Gastroc Mass Norm
Gastroc mass (mg/g initial BWg)

Figure 7

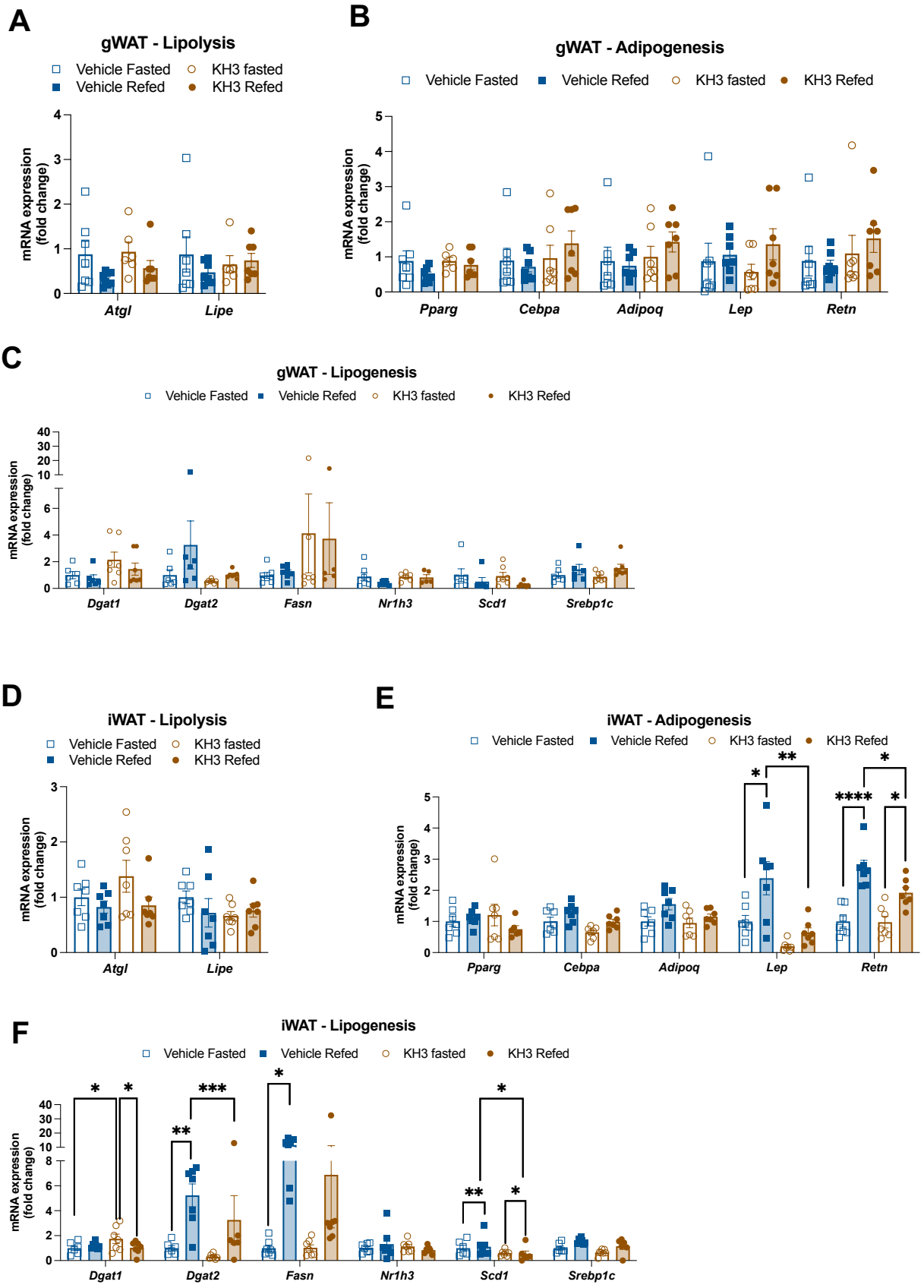
A
gWAT - Lipolysis
Vehicle Fasted
KH3 fasted
Vehicle Refed
KH3 Refed
mRNA expression (fold change)
Atgl
Lipe
B
gWAT - Adipogenesis
Vehicle Fasted
Vehicle Refed
KH3 fasted
KH3 Refed
mRNA expression (fold change)
Pparg
Cebpa
Adipoq
Lep
Retn
C
gWAT - Lipogenesis
Vehicle Fasted
Vehicle Refed
KH3 fasted
KH3 Refed
mRNA expression (fold change)
Dgat1
Dgat2
Fasn
Nr1h3
Scd1
Srebp1c
D
iWAT - Lipolysis
Vehicle Fasted
KH3 fasted
Vehicle Refed
KH3 Refed
mRNA expression (fold change)
Atgl
Lipe
E
iWAT - Adipogenesis
Vehicle Fasted
Vehicle Refed
KH3 fasted
KH3 Refed
mRNA expression (fold change)
Pparg
Cebpa
Adipoq
Lep
Retn
F
iWAT - Lipogenesis
Vehicle Fasted
Vehicle Refed
KH3 fasted
KH3 Refed
mRNA expression (fold change)
Dgat1
Dgat2
Fasn
Nr1h3
Scd1
Srebp1c

Figure 8